Open Journal of Fluid Dynamics, 2026, 16(3), 61-90
https://www.scirp.org/journal/ojfd
ISSN Online: 2165-3860
ISSN Print: 2165-3852

Analysis of the Linear Temporal Stability of Blood Flow under the Influence of a Magnetic Field in Microvessels

Toha François Lihonou[1,2*], Kalil Pierre Mathos[1], Hilaire Segning[2,3], Abdelghani Laouer[4], Casimir Raymond Tefo[1], Amoussou Laurent Hinvi[2,5]

[1]Department of Physics, Faculty of Science and Technology, University of N'Zerekore, Nzérékoré, Guinea
[2]LMFDNMSB Laboratory, IMSP/UAC, Porto-Novo, Benin
[3]Department of Fundamental Physics, ISSEG, Conakry, Guinea
[4]Department of Physics, Faculty of Exact Sciences and Computer Sciences, University of Jijel, Jijel, Algeria
[5]LaPIT Laboratory, UNSTIM, Abomey, Benin
Email: *lihonoulihonoutof@gmail.com

How to cite this paper: Lihonou, T.F., Mathos, K.P., Segning, H., Laouer, A., Tefo, C.R. and Hinvi, A.L. (2026) Analysis of the Linear Temporal Stability of Blood Flow under the Influence of a Magnetic Field in Microvessels. *Open Journal of Fluid Dynamics*, **16**, 61-90.
https://doi.org/10.4236/ojfd.2026.163005

Received: July 4, 2026
Accepted: September 7, 2026
Published: September 10, 2026

Abstract

In this work, we study the linear temporal stability of a unidirectional Poiseuille blood flow under the influence of the magnetic parameter and the Reynolds number. Blood is modeled as a spatially inhomogeneous fluid, with its viscosity dependent on the red blood cell concentration. We focus on small blood vessels, such as the terminal branches of arteries, arterioles, and small veins. For the basic flow, assumed to be laminar and two-dimensional, the basic velocity profiles were obtained numerically, including the magnetic effect, using the BVP4C method in Matlab. Stability analysis was performed using classical linear temporal analysis in terms of normal modes, leading to a fourth-order eigenvalue problem solved numerically using the Chebyshev spectral collocation method. The results indicate that the flow is unconditionally unstable. However, increasing the magnetic parameter or the Reynolds number, coupled with decreasing red blood cell concentration, reduces the degree of flow instability. The stabilization of blood flow in microvessels is essential for protecting the vascular walls.

Keywords

Linear Temporal Stability, Blood Flow, Microvessels, BVP4C Technique, Spectral Collocation Method

1. Introduction

Newtonian fluid theory describes the mechanical behavior of many real fluids with good accuracy. However, numerous fluids cannot be adequately described by this theory and are generally referred to as non-Newtonian fluids. Blood is one such non-Newtonian fluid and is the focus of the present study. It is a complex and heterogeneous fluid composed of red blood cells suspended in a liquid medium known as plasma. Microcirculation refers to the flow of blood through the smallest blood vessels, including capillaries, arterioles, and venules. It plays a crucial role in maintaining the proper functioning of tissues and organs, and any disruption of microcirculation can lead to serious health complications.

Haynes [1] investigated the inhomogeneity of blood resulting from the non-uniform distribution of red blood cells across the cross-sections of vessels with diameters smaller than 300 μm. In other words, during microcirculation, red blood cells are not uniformly distributed over the vessel cross-section; instead, they tend to accumulate near the vessel axis, thereby forming a cell-rich core and a cell-free layer adjacent to the vessel wall. Moyers-Gonzalez *et al.* [2] modeled blood as a suspension of red blood cells (RBCs) in a liquid phase (plasma). During blood microcirculation, the volume fraction of cells (hematocrit) varies across the vessel cross-section, a phenomenon known as the Fahraeus-Lindqvist effect [3]. The inhomogeneous distribution of red blood cells has significant implications for the rheological properties of blood, particularly its viscosity, which depends on the spatial distribution of the cells. Fournier [4] showed that the Fahraeus-Lindqvist effect modifies blood viscosity as a function of vessel diameter. This variation in viscosity can induce instabilities in blood flow, making certain concentration profiles more stable than others [5]. Therefore, linear stability analysis is essential for understanding how these instabilities develop and for identifying the flow patterns that are most likely to persist under physiological conditions.

In this study, we investigate the linear stability of unidirectional flow in a channel filled with a fluid whose viscosity is a positive function of the hematocrit. When the hematocrit is uniform across the cross-section, the fluid exhibits the constitutive behavior of a Newtonian fluid. Conversely, when the hematocrit varies across the vessel cross-section, the flow becomes inhomogeneous. Relevant studies on stratified flows include those dealing with the so-called central annular flow, *i.e.*, the parallel flow of two or more fluids with different viscosities. Blood flow in a microvessel, in connection with the Fahraeus-Lindqvist effect, is often modeled as a two-layer flow. Hickox [6] investigated the stability of this axisymmetric flow configuration, taking into account the effects of gravity and capillary forces acting at the interface between the two liquids. He showed that the steady Poiseuille flow of two immiscible fluids of different viscosities is unstable when the less viscous fluid is located at the center. Furthermore, Preziosi *et al.* [7] investigated more broadly the linear stability of the same basic flow by varying the viscosities, the volume ratios of the two fluids, and the Reynolds numbers. They showed that the flow is generally unstable, except when the less viscous fluid occupies the annular region, is sufficiently thin, and the Reynolds number lies within a limited range that depends on the fluid parameters. Anand and Rajagopal [5] demonstrated that inhomogeneous fluids, whose properties vary slightly from their mean values, can exhibit flow responses that differ by more than an order of magnitude from those associated with homogeneous fluids. Mohan Anand *et al.* [8] performed a linear stability analysis of a steady, fully developed flow of a shear-thinning fluid in a long cylindrical pipe. Using the shooting method, they found that all the computed eigenvalues are negative within the investigated Reynolds number range, indicating that the flow remains stable throughout this range. Miguel Moyers-Gonzalez *et al.* [2] applied the constitutive model originally proposed by Fang and Owens [9] and later developed by Owens [10] to steady, axisymmetric flow in rigid-walled tubes to describe non-homogeneous flows of healthy human blood. Their model accurately captures stress-induced cell migration in narrow tubes and predicts the Fahraeus-Lindqvist effect, according to which the apparent viscosity of healthy blood decreases with increasing tube diameter in sufficiently small vessels. Their numerical results show that this phenomenon is caused by the formation of a cell-depleted plasma layer near the vessel walls, which leads to a reduction in the tube hematocrit. Michela Ascolese *et al.* [3] showed that the marginal layer, although leading to a substantial reduction in flow resistance and an increase in discharge, does not decrease the energy dissipation rate. This result was obtained by considering six rheological models relating blood viscosity to hematocrit (the volume fraction occupied by erythrocytes). Lorenzo Fusi [11] studied the two-dimensional flow of a non-homogeneous incompressible fluid in a channel with a low aspect ratio. He extended the model to the case of a channel with variable thickness and compared his simulations with those obtained by Massoudi *et al.* [12]. Lorenzo Fusi *et al.* [13] studied the flow of a pressure-driven, inhomogeneous, incompressible thin film whose viscosity depends on its density. They showed that it is possible to determine an analytical solution to the problem when the boundary data are small perturbations of the homogeneous case. They then used this analytical solution to validate their numerical scheme. In [14], the authors illustrated the applications of mathematics to various physiological and artificial processes involving blood circulation, including hemorheology, microcirculation, coagulation, renal filtration, and dialysis, while providing a historical overview of each topic. They employed mathematical models to simulate processes occurring naturally in blood and to predict the effects of dysfunctions, such as coagulation disorders and renal failure, as well as the effects of therapies, to improve treatments. Khan A. *et al.* [15] presented a numerical study of the oscillatory motion of an Oldroyd-B fluid in a uniform magnetic field flowing through a small circular tube. First, they derived the orientation stress tensor by considering the Brownian force. Next, this tensor was incorporated into the Oldroyd-B model by considering Hookean dumbbells. The Oldroyd-B model was then reformulated by coupling it with the momentum equation and the total stress tensor. Finally, numerical simulations were performed to analyze the orientation stress tensor in the tube, showing that its effect is significant even when the Brownian force is sufficiently weak. According to Papalexandris [16] and Varsakelis *et al.*

[17], the constitutive modeling of non-Brownian particle suspensions is considerably more complex. Furthermore, particle deformability must also be taken into account when modeling blood. Indeed, Goldsmith *et al.* [18] and Moyers-Gonzalez *et al.* [19] showed that, for Stokes flow in tube suspensions, particle deformability strongly influences the flow behavior. They described the steady Poiseuille flow of blood in a small tube using a two-layer fluid model consisting of an outer plasma layer and an inner core in which blood is treated as a suspension of rouleaux of different sizes represented by deformable dumbbells (Moyers-Gonzalez *et al.* [2]). Consequently, the total stress is viscoelastic and consists of a small Newtonian contribution from the plasma and an elastic contribution from the red blood cells. Such an approach was employed by Dimakopoulos *et al.* [20] to simulate blood flow in a stenosed vessel. Gwennou Coupier *et al.* [21] experimentally and numerically investigated the non-inertial transverse migration of a vesicle in a confined Poiseuille flow. They observed that the combined effects of the vessel walls and the curvature of the velocity profile induce migration toward the centerline of the channel.

In [22], L. Fusi and A. Farina studied the linear stability of unidirectional Poiseuille blood flow, modeling the fluid as spatially inhomogeneous, with viscosity depending on the concentration of red blood cells (RBCs). Their work focused on small vessels—such as terminal arterial branches, arterioles, or venules—where the inhomogeneity arises from the non-uniform distribution of red blood cells across the vessel's cross-section. They found that distributions in which red blood cells are more concentrated near the vessel center are more "stable" than those in which red blood cells accumulate toward the vessel walls.

The objective and novelty of this work, compared to [22], lie in investigating the effect of a magnetic field and the Reynolds number on blood microcirculation through a linear temporal stability analysis, while—as in [22]—considering a hematocrit profile that depends only on the transverse coordinate, *i.e.*, stratified flows.

The effect of the magnetic field on flow stability was investigated by analyzing the linear temporal stability of a viscous, incompressible, and electrically conductive fluid forming a dynamic laminar boundary layer over an impermeable horizontal flat magnetic plate, as presented by Lihonou *et al.* [23]. John *et al.* [24] demonstrated that increasing the Reynolds number, through either a larger cylinder radius or a greater sweep angle, in the presence of wall suction, can stabilize the boundary layer at the leading edges of swept wings. This counterintuitive mechanism challenges conventional expectations regarding flow transition, showing that increasing certain parameters may, under specific conditions, have a stabilizing effect on the flow. Lebbal [25] showed that, for pulsatile flow, increasing the Reynolds number can temporally stabilize the eTWF modes.

To achieve our objective, we consider two classes of hematocrit profiles: one that increases monotonically across the vessel cross-section and another that decreases monotonically. We focus on flows at low Reynolds numbers because our primary interest lies in microcirculation, namely arteries, terminal branches, arterioles, and venules (*i.e.*, vessels with diameters ranging from 0.1 to 0.6 mm), where red blood cells are not uniformly distributed across the cross-section. To keep our analysis as general as possible, we employ three empirical laws relating blood viscosity to hematocrit. For each law, we determine the base velocity field corresponding to a prescribed transverse hematocrit profile. In particular, we examine two idealized cases representing the main hematocrit distributions: profiles that increase toward the vessel walls and profiles that decrease toward the vessel walls. Next, following the classical modal analysis of infinitesimal perturbations, we superimpose a small perturbation on the base flow and investigate its linear stability. The normal-mode formulation leads to a fourth-order eigenvalue problem, which is solved numerically using a Chebyshev polynomial method.

The remainder of this paper is organized as follows. In Section 2, we formulate the model for pressure-driven flow between two parallel plates. Section 3 presents the linear stability analysis, while Section 4 describes the numerical method used to solve the eigenvalue problem. The results and their discussion are presented in Section 5. Finally, concluding remarks are given in Section 6.

2. The Basic Flow

We consider a mechanically incompressible flow in a horizontal channel formed by two stationary parallel plates of length L^o, located at $y^o = -H^o$ and $y^o = +H^o$, giving a channel height of $2H^o$. The flow is driven by a prescribed pressure gradient G^o. A transverse magnetic field B^o, directed toward the positive y^o-axis, is applied across the channel. We exclude the cylindrical geometry, although it is physically more relevant, because it leads to a more involved numerical treatment. Likewise, the drag-driven flow case (*i.e.*, flow induced by the motion of a plate in the absence of a pressure gradient) is not considered, as it is less relevant to blood flow applications. The present study is therefore restricted to a two-dimensional configuration.

We chose to model the microvessels as a two-dimensional parallel-plate channel because this geometry eliminates variations along the third dimension, radically simplifying the Navier-Stokes equations to yield exact solutions for the velocity profile. It facilitates the assessment of wall shear stresses. However, this choice represents a limitation when extrapolating the results to actual cylindrical vessels.

The superscript $(.)^o$ denotes dimensional quantities or variables. We denote by

$$\boldsymbol{v}^o = u^o \boldsymbol{e}_x + v^o \boldsymbol{e}_y \tag{1}$$

the velocity field and we introduce the viscosity $\mu^o(\phi) = \mu_p^o \mu(\phi)$, where μ_p^o is a reference viscosity and $\mu(\phi)$ is dimensionless function. Assuming that the Cauchy stress tensor is given by $\mathbb{T}^o = -p^o \mathbb{I} + 2\mu^o(\phi)\mathbb{D}^o$, the mathematical formulation of the problem reads

$$\frac{\partial \phi}{\partial t^o} + \boldsymbol{v}^o \cdot \nabla^o \phi = 0, \tag{2}$$

$$\nabla^o \cdot \boldsymbol{v}^o = 0, \tag{3}$$

$$\rho^o \left(\frac{\partial \boldsymbol{v}^o}{\partial t^o} + \left(\boldsymbol{v}^o \cdot \nabla^o \right) \boldsymbol{v}^o \right) = -\nabla^o p^o + \mu_p^o \nabla^o \cdot \left(2\mu(\phi) \mathbb{D}^o \right) + J^o \wedge B, \tag{4}$$

$$\nabla^o \wedge B = \mu_e \left(J^o + \varepsilon_e E \right), \tag{5}$$

$$\nabla^o \wedge E = -\frac{\partial B}{\partial t^o}, \tag{6}$$

$$\nabla^o \cdot B = 0, \tag{7}$$

$$\nabla^o \cdot E = 0, \tag{8}$$

$$\nabla^o \cdot J^o = 0, \tag{9}$$

Equation (2) is a simple advection equation. Equation (3) and Equation (4) are continuity and Newton's second law respectively. Equations (5) - (9) are Ampere's law, Faraday's law, Maxwell's law and Gauss law equations respectively, with

$$J^o = \lambda \left(E + V^o \wedge B \right), \tag{10}$$

where ρ^o is the uniform fluid density, E the electric field, J^o the current density vector, μ_e the magnetic permeability, ε_e the absolute permittivity of the fluid, t^o the time, p^o the pressure, and λ is the Stefan-Boltzmann constant.

We also considered the following

$$B = \left(0, B_0, 0 \right), \tag{11}$$

$$E = \left(E_x, E_y, E_z \right), \tag{12}$$

$$J^o = \left(J_x^o, 0, J_z^o \right), \tag{13}$$

where B_0 is a constant. We assumed that no applied polarization voltage exists (*i.e.*, $E = 0$). Then Equation (10) and Equation (13) give

$$J^o = \lambda B_0 \left(-w^o, 0, u^o \right) \tag{14}$$

We rescale the problem with $x = \frac{x^o}{L^o}$, $y = \frac{y^o}{L^o}$, $H = \frac{H^o}{L^o}$, $U = \frac{u^o}{U^o}$, $V = \frac{v^o}{U^o}$, $p = \frac{p^o}{\rho^o {U^o}^2}$, $G = \frac{G^o L^o}{\rho^o {U^o}^2}$, where U^o is the characteristic velocity, still to be selected. The systems (2) - (4) becomes

$$\begin{cases} \frac{\partial \phi}{\partial t} + \boldsymbol{v} \cdot \nabla \phi = 0, \\ \nabla \cdot \boldsymbol{v} = 0, \\ \mathrm{Re}\left(\frac{\partial \boldsymbol{v}}{\partial t} + \left(\boldsymbol{v} \cdot \nabla \right) \boldsymbol{v} \right) = -\mathrm{Re} \nabla p + \nabla \cdot \left(2\mu(\phi) \mathbb{D} \right) + J \wedge B. \end{cases} \tag{15}$$

In Cartesian coordinates, we have:

$$\begin{cases} \dfrac{\partial \phi}{\partial t}+U\dfrac{\partial \phi}{\partial x}+V\dfrac{\partial \phi}{\partial y}=0 \\ \dfrac{\partial U}{\partial x}+\dfrac{\partial V}{\partial y}=0 \\ \mathrm{Re}\left(\dfrac{\partial U}{\partial t}+U\dfrac{\partial U}{\partial x}+V\dfrac{\partial U}{\partial y}\right)=-\mathrm{Re}\dfrac{\partial p}{\partial x}+\dfrac{\partial}{\partial x}\left(2\mu(\phi)\dfrac{\partial U}{\partial x}\right)+\dfrac{\partial}{\partial y}\left(\mu(\phi)\left(\dfrac{\partial U}{\partial y}+\dfrac{\partial V}{\partial x}\right)\right)-MU \\ \mathrm{Re}\left(\dfrac{\partial V}{\partial t}+U\dfrac{\partial V}{\partial x}+V\dfrac{\partial V}{\partial y}\right)=-\mathrm{Re}\dfrac{\partial p}{\partial y}+\dfrac{\partial}{\partial y}\left(2\mu(\phi)\dfrac{\partial V}{\partial y}\right)+\dfrac{\partial}{\partial x}\left(\mu(\phi)\left(\dfrac{\partial U}{\partial y}+\dfrac{\partial V}{\partial x}\right)\right) \end{cases} \tag{16}$$

where $\mathrm{Re}=L^oU^o/\mu_p^o$ is the Reynolds number and $M=\lambda B_0^2L^{o^2}/\mu_p^o$, the magnetic parameter. We then look for a basic flow of the type $U=U(y)$, $V=0$, $p=p_o(x)$, $\phi=\phi_o(y)$, satisfying the boundary conditions

$$U(H)=0,\ \frac{\partial U}{\partial y}(0)=0,\ p_o(0)=p_{in},\ p_o(1)=p_{in}-G, \tag{17}$$

where p_{in} is the dimensionless inlet pressure.
we set:

$$\mu(\phi)=\mu_o(\phi).$$

So the system becomes:

$$\begin{cases} 0=-\mathrm{Re}\dfrac{\partial p_o}{\partial x}+\dfrac{\partial}{\partial y}\left(\mu_o(\phi)\left(\dfrac{\partial U}{\partial y}\right)\right)-MU \\ 0=\dfrac{\partial}{\partial x}\left(\mu_o(\phi)\left(\dfrac{\partial U}{\partial y}\right)\right) \end{cases} \tag{18}$$

The base flow rate is evaluated in the lower half of the channel, the upper half being obtained by symmetry.

Considering the first equation of system (18), we obtain

$$\frac{\partial}{\partial y}\left(\mu_o(\phi)\frac{\partial U(y)}{\partial y}\right)-MU=\mathrm{Re}\frac{\partial P_o}{\partial x}$$

considered the following

$$p_o(x)=-Gx+p_{in},$$

this leads $\dfrac{\partial P_o}{\partial x}=-G$

We therefore obtain:

$$\frac{\partial}{\partial y}\left(\mu_o(\phi)\frac{\partial U(y)}{\partial y}\right)-MU=-\mathrm{Re}\,G. \tag{19}$$

We considered:

$$\mathrm{Re}\,G\int_0^H\frac{\zeta}{\mu_o(\zeta)}\mathrm{d}\zeta=1, \tag{20}$$

Thus, the Equation (19) can be written in the form:

$$\mu_o U'' + \dot{\mu}_o \phi' U' - MU + \frac{1}{\int_0^H \frac{y}{\mu_o(y)} \mathrm{d}y} = 0, \tag{21}$$

where

$$\operatorname{Re} G = \frac{1}{\int_0^H \frac{y}{\mu_o(y)} \mathrm{d}y} \tag{22}$$

$$\left.\frac{\mathrm{d}\mu_o(\phi)}{\mathrm{d}\phi}\right|_{\phi=\phi_0(y)} = \dot{\mu}_o(y),$$

$$\frac{\mathrm{d}\phi}{\mathrm{d}y} = \phi',$$

The boundary conditions are:

$$U(\pm H) = 0,\ U'(0) = 0. \tag{23}$$

Furthermore, we take:

$$\phi(y) = \frac{\phi_M \phi_m}{(1-y^2)\phi_m + y^2 \phi_M} \tag{24}$$

In (24) $\phi_m = 0.1, \phi_M = 0.7$ are the minimum and maximum values attained by the hematocrit .

Thus, the hematocrit functions become:

$$\phi(y) = \frac{0.07}{(0.1 + 0.6y^2)}$$

$$\phi'(y) = \frac{-0.084y}{(0.1 + 0.6y^2)^2}$$

Such a choice of $\phi_o(y)$ does not correspond to any real physiological situation; however, it provides a regular symmetric function bounded between two reasonable hematocrit values and attaining its maximum at ($y = 0$). We recall that the hematocrit ϕ_o varies locally, thereby affecting the viscous stress, while the fluid density remains unchanged.

In the literature, numerous empirical formulas have been proposed to relate viscosity to hematocrit (see, for instance, Fournier [4] and Hund *et al.* [26]). All these formulas share the common feature that μ_o is an increasing function of ϕ. In the present work, we consider some of the most commonly used expressions reported in the literature, namely those proposed by Hatschek [27], Cokelet [28], and Nubar [29]:

$$\mu(\phi) = \frac{1}{1-\phi^{1/3}}, \text{ (Hatschek [27])} \tag{25}$$

either:

$$\dot{\mu} = \frac{1}{3\left(\phi^{1/3} - \phi^{2/3}\right)^2}, \tag{26}$$

$$\mu(\phi)=\frac{1}{(1-\phi)^{2.5}}, \text{ (Cokelet [28])} \tag{27}$$

either:

$$\dot{\mu}=\frac{2.5\phi^{1.5}}{(1-\phi)^{5}}, \tag{28}$$

$$\mu(\phi)=\frac{0.75}{0.75-\phi}, \text{ (Nubar [29])} \tag{29}$$

either:

$$\dot{\mu}=\frac{0.75}{(0.75-\phi)^{2}}. \tag{30}$$

3. Linear Stability Analysis

To carry out a linear stability analysis of the basic flow (19), we introduce the following perturbed solution:

$$\left[u-U(y),v,p-p_o(x),\phi-\phi_o(y)\right]=\left[\hat{u}(y),\hat{v}(y),\hat{p}(y),\hat{\phi}(y)\right]\mathrm{e}^{i(\alpha x-\omega t)} \tag{31}$$

e.i.

$$\begin{aligned}
u(x,y,t)&=U(y)+\hat{u}(y)\mathrm{e}^{i(\alpha x-\omega t)},\\
v(x,y,t)&=\hat{v}(y)\mathrm{e}^{i(\alpha x-\omega t)},\\
p(x,y,t)&=p_o(x)+\hat{p}(y)\mathrm{e}^{i(\alpha x-\omega t)},\\
\phi(x,y,t)&=\phi_o(y)+\hat{\phi}(y)\mathrm{e}^{i(\alpha x-\omega t)},
\end{aligned}$$

where $|\hat{\cdot}|\ll 1$, $\alpha\in\mathbb{R}$ is the wave number and $\omega\in\mathbb{C}$ is the frequency. Introducing

$$c=\frac{\omega}{\alpha},\ \text{with } c\in\mathbb{C},$$

the perturbation phase can be rewritten as

$$i(\alpha x-\omega t)=i\alpha(x-ct).$$

Setting

$$\left.\frac{\mathrm{d}\mu(\phi)}{\mathrm{d}\phi}\right|_{\phi=\phi_o(y)}=\dot{\mu}_o(y), \tag{32}$$

By expanding the viscosity function in the vicinity of ϕ_o up to the linear term, one successively obtains:

$$\mu(\phi(x,y,t))=\mu(\phi_o)+\frac{(\phi-\phi_o)}{1!}\left.\frac{\mathrm{d}\mu}{\mathrm{d}\phi}\right|_{\phi=\phi_o}$$

$$\mu(\phi_o)=\mu_o(y);\left.\frac{\mathrm{d}\mu}{\mathrm{d}\phi}\right|_{\phi=\phi_o}=\dot{\mu}_o\ \text{ and }\ \phi-\phi_o=\hat{\phi}(y)\mathrm{e}^{i(\alpha x-\omega t)}$$

Then, the viscosity function is expanded up to the linear term as follows:

$$\mu(\phi(x,y,t)) = \mu_o(y) + \dot{\mu}_o(y)\hat{\phi}(y)\mathrm{e}^{i(\alpha x-\omega t)}, \tag{33}$$

By substituting Eqs. (31) into $(15)_1$, we have:

$$\frac{\partial}{\partial t}\left[\hat{\phi}\mathrm{e}^{i(\alpha x-\omega t)}\right] + \left[U(y)+\hat{u}(y)\mathrm{e}^{i(\alpha x-\omega t)}\right]\frac{\partial}{\partial x}\left[\phi_o(y)+\hat{\phi}\mathrm{e}^{i(\alpha x-\omega t)}\right]$$
$$+\left(\hat{v}\mathrm{e}^{i(\alpha x-\omega t)}\right)\frac{\partial}{\partial y}\left[\phi_o(y)+\hat{\phi}\mathrm{e}^{i(\alpha x-\omega t)}\right] = 0.$$

Since $\dfrac{\partial \phi}{\partial t} = \dfrac{\partial}{\partial t}\left[\phi_o(y)+\hat{\phi}\mathrm{e}^{i(\alpha x-\omega t)}\right] = \dfrac{\partial \phi_o(y)}{\partial t} + \dfrac{\partial}{\partial t}\left(\hat{\phi}(y)\mathrm{e}^{i(\alpha x-\omega t)}\right)$ and $\dfrac{\partial \phi_o(y)}{\partial t} = 0$, then

$$\frac{\partial \phi}{\partial t} = -i\omega\hat{\phi}(y)\mathrm{e}^{i(\alpha x-\omega t)}$$

Similarly, $\dfrac{\partial \phi}{\partial x} = \dfrac{\partial}{\partial x}\left[\phi_o(y)+\hat{\phi}(y)\mathrm{e}^{i(\alpha x-\omega t)}\right] = \dfrac{\partial \phi(y)}{\partial x} + \dfrac{\partial}{\partial x}\left[\hat{\phi}(y)\mathrm{e}^{i(\alpha x-\omega t)}\right]$ with $\dfrac{\partial \phi_o(y)}{\partial x} = 0$. Then

$$\frac{\partial \phi}{\partial x} = i\alpha\hat{\phi}(y)\mathrm{e}^{i(\alpha x-\omega t)}$$

At the same time, we have:

$\dfrac{\partial \phi}{\partial y} = \dfrac{\mathrm{d}\phi_o(y)}{\mathrm{d}y} + \dfrac{\partial}{\partial y}\left[\hat{\phi}(y)\mathrm{e}^{i(\alpha x-\omega t)}\right] = \dfrac{\mathrm{d}\phi_o(y)}{\mathrm{d}y} + \dfrac{\mathrm{d}\hat{\phi}(y)}{\mathrm{d}y}\mathrm{e}^{i(\alpha x-\omega t)}$, e.i.:

$$\frac{\partial \phi}{\partial y} = \phi_o'(y) + \hat{\phi}(y)\mathrm{e}^{i(\alpha x-\omega t)}$$

Equation $(15)_1$ successively becomes:

$$i\omega\hat{\phi}(y)\mathrm{e}^{i(\alpha x-\omega t)} + \left[U(y)+\hat{u}(y)\mathrm{e}^{i(\alpha x-\omega t)}\right]\left[i\alpha\hat{\phi}(y)\mathrm{e}^{i(\alpha x-\omega t)}\right]$$
$$+\hat{v}(y)\mathrm{e}^{i(\alpha x-\omega t)}\left[\phi_o'(y)+\hat{\phi}_o'(y)\mathrm{e}^{i(\alpha x-\omega t)}\right] = 0$$

$$i\omega\hat{\phi}(y) + i\alpha\hat{\phi}(y)U(y) + i\alpha\hat{u}(y)\hat{\phi}(y)\mathrm{e}^{i(\alpha x-\omega t)} + \hat{v}(y)\phi_o'(y)$$
$$+\hat{v}(y)\hat{\phi}_o'(y)\mathrm{e}^{i(\alpha x-\omega t)} = 0$$

$$i(\alpha U-\omega)\hat{\phi}(y) + \hat{v}(y)\phi_o'(y) + i\alpha\hat{u}(y)\hat{\phi}'(y)\mathrm{e}^{i(\alpha x-\omega t)} + \hat{v}(y)\hat{\phi}'(y)\mathrm{e}^{i(\alpha x-\omega t)} = 0$$

Neglecting the nonlinear terms, we obtain

$$i(\alpha U-\omega)\hat{\phi} + \hat{v}\phi_o' = 0 \tag{34}$$

By substituting Eqs. (31) into $(15)_2$, we have:

$$\frac{\partial u}{\partial x} + \frac{\partial v}{\partial y} = i\alpha\hat{u}(y)\mathrm{e}^{i(\alpha x-\omega t)} + \frac{\mathrm{d}\hat{v}(y)}{\mathrm{d}y}\mathrm{e}^{i(\alpha x-\omega t)} = 0$$

with $\dfrac{\partial U(y)}{\partial x} = 0$

Equation $(15)_2$ successively becomes:

$$i\alpha\hat{u}(y)\mathrm{e}^{i(\alpha x-\omega t)} + \hat{v}'(y)\mathrm{e}^{i(\alpha x-\omega t)} = 0$$

$$\hat{v}' + i\alpha\hat{u} = 0, \tag{35}$$

where

$$(\cdot)' = \frac{\mathrm{d}(\cdot)}{\mathrm{d}y}.$$

Substituting (31) and (33) into $(15)_3$ we obtain

$$\mathrm{Re}\left(\frac{\partial u}{\partial t}+u\frac{\partial u}{\partial x}+v\frac{\partial u}{\partial y}\right)=-\mathrm{Re}\frac{\partial p}{\partial x}+\frac{\partial}{\partial x}\left(2\mu(\phi)\frac{\partial u}{\partial x}\right)+\frac{\partial}{\partial y}\left[\mu(\phi)\left(\frac{\partial u}{\partial y}+\frac{\partial v}{\partial x}\right)\right]-Mu$$

and

$$\mathrm{Re}\left(\frac{\partial v}{\partial t}+u\frac{\partial v}{\partial x}+v\frac{\partial v}{\partial y}\right)=-\mathrm{Re}\frac{\partial p}{\partial y}+\frac{\partial}{\partial y}\left[2\mu(\phi)\frac{\partial v}{\partial y}\right]+\frac{\partial}{\partial x}\left[\mu(\phi)\left(\frac{\partial u}{\partial y}+\frac{\partial v}{\partial x}\right)\right]$$

We can calculate:

$$\frac{\partial\mu(\phi)}{\partial x}=i\alpha\dot{\mu}_o\hat{\phi}(y)\mathrm{e}^{i(\alpha x-\omega t)},$$

$$\frac{\partial}{\partial x}\left[2\mu(\phi)\frac{\partial u}{\partial x}\right]=2\frac{\partial\mu(\phi)}{\partial x}\frac{\partial u}{\partial x}+2\mu(\phi)\frac{\partial^2 u}{\partial x^2}$$

$$\frac{\partial}{\partial x}\left[2\mu(\phi)\frac{\partial u}{\partial x}\right]=-2\alpha^2\dot{\mu}_o\hat{\phi}\hat{u}\mathrm{e}^{2i(\alpha x-\omega t)}-2\alpha^2\mu_o\hat{u}\mathrm{e}^{i(\alpha x-\omega t)}-2\alpha^2\dot{\mu}_o\hat{u}\hat{\phi}\mathrm{e}^{2i(\alpha x-\omega t)},$$

$$\frac{\partial}{\partial y}\left[\mu(\phi)\left(\frac{\partial u}{\partial y}+\frac{\partial v}{\partial x}\right)\right]$$

$$=\frac{\partial}{\partial y}\left[\mu_o U'+\dot{\mu}U'\hat{\phi}\mathrm{e}^{i(\alpha x-\omega t)}+\mu_o\left(\hat{u}'+i\alpha\hat{v}\right)\mathrm{e}^{i(\alpha x-\omega t)}+\dot{\mu}_o\hat{\phi}\left(\hat{\mu}'+i\alpha\hat{v}\right)\mathrm{e}^{i(\alpha x-\omega t)}\right]$$

$$\frac{\partial}{\partial y}\left[2\mu(\phi)\frac{\partial v}{\partial y}\right]=2\frac{\partial\mu(\phi)}{\partial y}\frac{\partial v}{\partial y}+2\mu(\phi)\frac{\partial^2 v}{\partial y^2}$$

$$\frac{\partial}{\partial y}\left[2\mu(\phi)\frac{\partial v}{\partial y}\right]=2U'\hat{v}'\mathrm{e}^{i(\alpha x-\omega t)}+2\dot{\mu}_o'\hat{v}'\hat{\phi}\mathrm{e}^{2i(\alpha x-\omega t)}+2\dot{\mu}_o\hat{v}'\hat{\phi}'\mathrm{e}^{2i(\alpha x-\omega t)}$$
$$+2\mu_o\hat{v}''\mathrm{e}^{i(\alpha x-\omega t)}+2\dot{\mu}_o\hat{\phi}\hat{v}''\mathrm{e}^{i(\alpha x-\omega t)}$$

$$\frac{\partial}{\partial y}\left[2\mu(\phi)\frac{\partial v}{\partial y}\right]=\frac{\mathrm{d}}{\mathrm{d}y}\left(2\mu_o\hat{v}'\right)\mathrm{e}^{i(\alpha x-\omega t)}+2\dot{\mu}_o\hat{v}'\hat{\phi}\mathrm{e}^{2i(\alpha x-\omega t)}$$
$$+2\dot{\mu}_o\hat{v}'\hat{\phi}'\mathrm{e}^{2i(\alpha x-\omega t)}+2\dot{\mu}_o\hat{\phi}\hat{v}''\mathrm{e}^{i(\alpha x-\omega t)}$$

$$\frac{\partial}{\partial x}\left[\mu(\phi)\left(\frac{\partial u}{\partial y}+\frac{\partial v}{\partial x}\right)\right]=\frac{\partial}{\partial x}\left(\mu_o U'\right)+\left[\dot{\mu}_o\hat{\phi}U'\mathrm{e}^{i(\alpha x-\omega t)}+\mu_o\left(\hat{u}'+i\alpha\hat{v}\right)\mathrm{e}^{i(\alpha x-\omega t)}\right.$$
$$\left.+\dot{\mu}_o\hat{\phi}\left(\hat{u}'+i\alpha\hat{v}\right)\mathrm{e}^{i(\alpha x-\omega t)}\right]$$

Thus, along (x) and (y), the equation $(15)_3$ becomes:

$$\mathrm{Re}\left[-i\omega\hat{u}\mathrm{e}^{i(\alpha x-\omega t)}+\left(\mu_o+\hat{u}\mathrm{e}^{i(\alpha x-\omega t)}\right)\left(i\alpha\hat{u}\mathrm{e}^{i(\alpha x-\omega t)}\right)+\left(\hat{v}\mathrm{e}^{i(\alpha x-\omega t)}\right)\left(\mu_o'+\hat{u}'\mathrm{e}^{i(\alpha x-\omega t)}\right)\right]$$

$$=-\mathrm{Re}\left(\frac{\partial p_o(x)}{\partial x}+i\hat{p}\mathrm{e}^{i(\alpha x-\omega t)}\right)-2\alpha^2\dot{\mu}_o\hat{u}\hat{\phi}\mathrm{e}^{2i(\alpha x-\omega t)}-2a^2\mu_o\hat{u}\mathrm{e}^{i(\alpha x-\omega t)}-2\alpha^2\dot{\mu}_o\hat{u}\hat{\phi}\mathrm{e}^{i(\alpha x-\omega t)}$$

$$+\frac{\partial}{\partial y}\left[\mu_o U'+\dot{\mu}_o U'\hat{\phi}\mathrm{e}^{i(\alpha x-\omega t)}+\mu_o\left(\hat{u}'+i\alpha\hat{v}\right)\mathrm{e}^{i(\alpha x-\omega t)}+\dot{\mu}_o\hat{\phi}\left(\hat{u}'+i\alpha\hat{v}\right)\mathrm{e}^{2i(\alpha x-\omega t)}\right]$$

$$-MU-M\hat{u}\mathrm{e}^{i(\alpha x-\omega t)}$$

and

$$\begin{aligned}&\mathrm{Re}\Big[-i\omega\hat{v}\mathrm{e}^{i(\alpha x-\omega t)}+\Big(U+\hat{u}\mathrm{e}^{i(\alpha x-\omega t)}\Big)\Big(i\alpha\hat{v}\mathrm{e}^{i(\alpha x-\omega t)}\Big)\Big(\hat{v}'\mathrm{e}^{i(\alpha x-\omega t)}\Big)\Big]\\&=-\mathrm{Re}\,\hat{p}'\mathrm{e}^{i(\alpha x-\omega t)}+\frac{\mathrm{d}}{\mathrm{d}y}\big(2\mu_o\hat{v}'\big)\mathrm{e}^{i(\alpha x-\omega t)}+2\dot{\mu}_o'\hat{v}'\hat{\phi}\mathrm{e}^{2i(\alpha x-\omega t)}\\&\quad+2\dot{\mu}_o\hat{v}'\hat{\phi}'\mathrm{e}^{2i(\alpha x-\omega t)}+2\dot{\mu}_o\hat{\phi}\hat{v}''\mathrm{e}^{i(\alpha x-\omega t)}+\frac{\partial}{\partial x}\big(\mu_oU'\big)\\&\quad+i\alpha\Big[\dot{\mu}_o\hat{\phi}U'\mathrm{e}^{i(\alpha x-\omega t)}+\mu_o\big(\hat{u}'+i\alpha\hat{v}\big)\mathrm{e}^{i(\alpha x-\omega t)}+\dot{\mu}_o\hat{\phi}\big(\hat{u}'+i\alpha\hat{v}\big)\mathrm{e}^{i(\alpha x-\omega t)}\Big].\end{aligned}$$

Based on the base flow, we have:

$$-\mathrm{Re}\frac{\partial p_o(x)}{\partial x}+\frac{\partial}{\partial y}\big(\mu_oU'\big)-MU=0$$

and $\dfrac{\partial}{\partial x}\big(\mu_oU'\big)=0$

Furthermore, by neglecting the non-linear terms and simplifying the exponential function in these preceding equations of motion, we obtain:

$$\mathrm{Re}\big(-i\omega\hat{u}+i\alpha U\hat{u}+U'\hat{v}\big)=-i\alpha\,\mathrm{Re}\,\hat{p}-2\alpha^2\mu_o\hat{u}+\frac{\mathrm{d}}{\mathrm{d}y}\Big[\mu_o\big(\hat{u}'+i\alpha\hat{v}\big)+\dot{\mu}_o\hat{\phi}U'\Big]-M\hat{u}\quad(36)$$

and

$$\mathrm{Re}\big(-i\omega\hat{v}+i\alpha U\hat{v}\big)=-\mathrm{Re}\,\hat{p}'+i\alpha\Big(\mu_o\big(\hat{u}'+i\alpha\hat{v}\big)+\dot{\mu}_o\hat{\phi}U'\Big)+\frac{\mathrm{d}}{\mathrm{d}y}\big[2\mu_o\hat{v}'\big]\quad(37)$$

Exploiting (35) and introducing

$$Q(y)=\mu_o(y)-1,$$
$$P(y)=\dot{\mu}_o(y)\phi_o'(y)U'(y),$$

Equation (36) and Equation (37) can be rewritten as

$$\begin{aligned}&\mathrm{Re}\big(-i\omega\hat{u}+i\alpha U\hat{u}+U'\hat{v}\big)\\&=-i\alpha\,\mathrm{Re}\,\hat{p}-2\alpha^2Q\hat{u}+\left(\frac{\mathrm{d}^2}{\mathrm{d}y^2}-\alpha^2\right)\hat{u}+\frac{\mathrm{d}}{\mathrm{d}y}\left[Q\big(\hat{u}'+i\alpha\hat{v}\big)+P\frac{\hat{\phi}}{\phi_o'}\right]-M\hat{u}\end{aligned}\quad(38)$$

$$\mathrm{Re}\big(-i\omega\hat{v}+i\alpha U\hat{v}\big)=-\mathrm{Re}\,\hat{p}'+\left(\frac{\mathrm{d}^2}{\mathrm{d}y^2}-\alpha^2\right)\hat{v}+i\alpha\left[Q\big(\hat{u}'+i\alpha\hat{v}\big)+P\frac{\hat{\phi}}{\phi_o'}\right]+\frac{\mathrm{d}}{\mathrm{d}y}\big[2Q\hat{v}'\big]\quad(39)$$

Eliminating the pressure between Equation (38) and Equation (39) and using Equation (35), we obtain

$$\begin{aligned}&\mathrm{Re}\big[i(\alpha U-\omega)\big(\hat{u}'-i\alpha\hat{v}\big)+U''\hat{v}\big]\\&=\left(\frac{\mathrm{d}^2}{\mathrm{d}y^2}-\alpha^2\right)\big(\hat{u}'-i\alpha\hat{v}\big)+\left(\frac{\mathrm{d}^2}{\mathrm{d}y^2}+\alpha^2\right)\left[Q\big(\hat{u}'+i\alpha\hat{v}\big)+P\frac{\hat{\phi}}{\phi_o'}\right]\\&\quad-2i\alpha\frac{\mathrm{d}}{\mathrm{d}y}\big[Q\big(\hat{v}'-i\alpha\hat{u}\big)\big]-M\hat{u}'\end{aligned}\quad(40)$$

Introducing the new variable $f(y)$

$$\hat{\phi}=\phi_o'f,$$

implying that $\hat{\phi}$ is symmetric with respect to $y=0$, Equation (34) and Equation (35) can be rewritten as

$$\hat{v} = i\alpha\left(c-U\right)f,\ \hat{u} = -\frac{\mathrm{d}}{\mathrm{d}y}\left[\left(c-U\right)f\right].$$

We also have:

$$\hat{v}' = i\alpha\frac{\mathrm{d}}{\mathrm{d}y}\left[\left(c-U\right)f\right],\ \hat{u}' = -\frac{\mathrm{d}^2}{\mathrm{d}y^2}\left[\left(c-U\right)f\right].$$

On substituting the above into Equation (40) we obtain the fourth order eigenvalue problem

$$\begin{aligned} & i\alpha\,\mathrm{Re}\left\{(U-c)\left(\mathrm{D}^2-\alpha^2\right)-U''\right\}\left[(U-c)f\right] \\ & =\left(\mathrm{D}^2-\alpha^2\right)^2\left[(U-c)f\right]+\left(\mathrm{D}^2+\alpha^2\right)\left\{Q\left(\mathrm{D}^2+\alpha^2\right)\left[(U-c)f\right]+Pf\right\} \\ & \quad -4\alpha^2\mathrm{D}\left\{Q\mathrm{D}\left[(U-c)f\right]\right\}-M\mathrm{D}^2\left[(U-c)f\right] \end{aligned} \tag{41}$$

where

$$\mathrm{D}^k = \frac{\mathrm{d}^k}{\mathrm{d}y^k}$$

and whose boundary conditions are

$$f\big|_{\pm H} = 0,\ \ f'\big|_{\pm H} = 0. \tag{42}$$

System (41) and (42) provides the eigenvalues $c\in\mathbb{C}$, and the relative eigenfunctions f, that allows one to establish if the basic flow, corresponding to the prescribed ϕ_o and to the selected $\mu_o(\phi)$, is linearly stable or not. In particular, when $\mathrm{Im}(c)>0$ the system is unstable.

Remark 1. We observe that when $Q=P=0$, *i.e.* when $\mu=1$, setting $g=(U-c)f$, the Equation (41) become:

$$i\alpha\,\mathrm{Re}\left\{(U-c)\left(\mathrm{D}^2-\alpha^2\right)-U''\right\}g=\left(\mathrm{D}^2-\alpha^2\right)^2 g-M\mathrm{D}^2 g.$$

Furthermore, when the magnetic parameter (*M*) is set to zero, the classical Orr-Sommerfeld equation is recovered

$$i\alpha\,\mathrm{Re}\left\{(U-c)\left(\mathrm{D}^2-\alpha^2\right)-U''\right\}g=\left(\mathrm{D}^2-\alpha^2\right)^2 g.$$

The aim here is not to solve the classical Orr-Sommerfeld equation, but rather to solve the complex Equation (41); we will first transform this into an eigenvalue equation, enabling a direct analysis of blood flow stability, simplifying the calculation of perturbation waves, and allowing the use of appropriate numerical methods.

To expand Equation (41) by letting the operator D act on its contents, let us set:

$$\Gamma_L = i\alpha\,\mathrm{Re}\left\{(U-c)\left(\mathrm{D}^2-\alpha^2\right)-U''\right\}\left[(U-c)f\right], \text{ and}$$

$$\begin{aligned} \Gamma_R = & \left(\mathrm{D}^2-\alpha^2\right)^2\left[(U-c)f\right]+\left(\mathrm{D}^2+\alpha^2\right)\left\{Q\left(\mathrm{D}^2+\alpha^2\right)\left[(U-c)f\right]+Pf\right\} \\ & -4\alpha^2\mathrm{D}\left\{Q\mathrm{D}\left[(U-c)f\right]\right\}-M\mathrm{D}^2\left[(U-c)f\right] \end{aligned}$$

Thus, we have:

$$\Gamma_L = \left[i\alpha \operatorname{Re} UU''f + i\alpha \operatorname{Re} U^2 D^2 f + 2i\alpha \operatorname{Re} UU'Df - i\alpha^3 \operatorname{Re} U^2 f - i\alpha \operatorname{Re} UU''f \right]$$
$$+ c\left[-i\alpha \operatorname{Re} UD^2 f + 2i\alpha^3 \operatorname{Re} Uf - i\alpha \operatorname{Re} U''f - i\alpha \operatorname{Re} UD^2 f - 2i \operatorname{Re} U'Df \right.$$
$$\left. + i\alpha \operatorname{Re} U''f \right] + c^2\left[i\alpha \operatorname{Re} D^2 f \right.$$

and

$$\Gamma_R = -4\alpha^2 Q'U''f - 4\alpha^2 Q'UD^2 f - 8\alpha^2 Q'U'Df + 4c\alpha^2 Q'Df - 4\alpha^2 QU^{(3)} f$$
$$- 4\alpha^2 QU''Df - 4\alpha^2 QU'D - 4\alpha^2 QUD^3 f - 8\alpha^2 QU''Df - 8\alpha^2 QU'D^2 f$$
$$+ 4a^2 QcD^2 f + \alpha^4 Uf - \alpha^4 cf + UD^4 f + 4U'D^3 f + 4U^{(3)}Df + U^{(4)} f$$
$$- cD^4 f - 2\alpha^2 U''f - 2\alpha^2 UD^2 f - 4\alpha^2 U'Df + 2\alpha^2 cD^2 f + \alpha^2 QU''f$$
$$+ \alpha^2 QUf + 2\alpha^2 QU'Df - c\alpha^2 QD^2 f + \alpha^4 QUf - c\alpha^4 Qf + \alpha^2 Pf + P''f$$
$$+ PD^2 f + 2P'Df - c\alpha^2 Q''f - c - 2c\alpha^2 Q'Df - cQ''D^2 f - cQD^4 f$$
$$- cQ'D^3 f + Q''U''f + QU^{(4)} f + QU''D^2 f + 2Q'U^{(3)} f + 2QU + 2Q'U''Df$$
$$+ Q''UD^2 f + QU''D^2 f + QUD^4 f + 2Q'U'D^2 f + 2QU'D^3 f + 2Q'UD^3 f$$
$$+ 2Q''U' + 2QU'D^3 f + 4Q'U''Df + 4QU'' + 4Q'U'D^2 f + \alpha Q''Uf$$
$$+ a^2 QU''f + \alpha^2 QUD^2 f + 2\alpha^2 Q'U' + 2\alpha^2 QU'Df + 2\alpha^2 Q'UDf - MU''f$$
$$- 2MU'Df - MUD^2 f + cMD^2 f$$

By taking

$$\Gamma_L - \Gamma_R = 0$$

and then factoring the c, Equation (41) can be rewritten as

$$\Gamma_0 f + c\Gamma_1 f + c^2 \Gamma_2 f = 0, \tag{43}$$

where Γ_j are the differential operators

$$\Gamma_j = \sum_{k=0}^{4} \Gamma_{jk}(y) D^k. \tag{44}$$

The coefficients $\Gamma_{jk}(y)$ are reported in **Appendix**.

So,

$$\Gamma_0 = \Gamma_{00} + \Gamma_{01} D + \Gamma_{02} D^2 + \Gamma_{03} D^3 + \Gamma_{04} D^4, \tag{45}$$

$$\Gamma_1 = \Gamma_{10} + \Gamma_{11} D + \Gamma_{12} D^2 + \Gamma_{13} D^3 + \Gamma_{14} D^4, \tag{46}$$

$$\Gamma_2 = \Gamma_{20} + \Gamma_{21} D + \Gamma_{22} D^2 + \Gamma_{23} D^3 + \Gamma_{24} D^4. \tag{47}$$

4. Numerical Solution Method

4.1. Basic Flow Solution Method

For the numerical solution of the basic flow, we employed the bvp4c solver implemented in MATLAB, following the approach of Shampine *et al.* [30]. This method has also been used by T. Jamir and H. Konwar (2022) [31] and by Lihonou *et al.* (2025) [32] [33]. Therefore, the highly coupled nonlinear ordinary differential Equation (21), together with the boundary conditions (23), is solved by introducing the following variables:

$$A1 = (Ip * gp)/I\ ;$$

$$A2 = M/I\ ;$$

$$A3 = RG/I\ ;$$

$$U = Z_1;\ \ U' = Z_2\ ;$$

$U'' = Z_2' = -A1 * Z_2 + A2 * Z_1 - A3$; where gp is the derivative of the hematocrit function; I is the viscosity function and Ip is the derivative of the viscosity function. RG represents the function (22).

For $y = \pm 1$, $Z_1 = 0$;

for $y = 0$, $Z_2 = 0$.

4.2. Perturbation Flow Solution Method

This subsection is devoted to the numerical solution of problems (41) and (42). The main objective is to determine the eigenvalue with the largest imaginary part as a function of the wave number α for different values of the magnetic parameter. We therefore define:

$$\sigma = \max_{c \in \Sigma} \operatorname{Im}(c),$$

where Σ is the spectrum of the system (41) and (42). For simplicity, we assume that the channel length and its half-amplitude are equal, so that $H = 1$, and that the channel walls have a height $y = \pm 1$.

Concerning the hematocrit profile $\phi_o(y)$, we select

$$\phi_o(y) = ey^2 + b, \tag{48}$$

where $b \in [0,1]$ and $-b < e < 1 - b$, so that $\phi_o(y) \in [0,1]$ when $y \in [-1,1]$. In particular, we consider two cases:

1) $e > 0$, the hematocrit is larger at the channel walls and so is the viscosity (which is an increasing function of the hematocrit).

2) $e < 0$, the RBCs concentration is larger in the middle of the channel and so is viscosity.

As a preliminary case we consider a simple linear model for μ_o

$$\mu_o(\phi) = T\phi + 1, \text{ with } T > 0, \tag{49}$$

which, combined with (48), gives

$$\mu_o(y) = eTy^2 + (bT + 1). \tag{50}$$

We take the explicit expression of the velocity profile

$$U(y) = 1 - \Lambda \ln(\beta y^2 + 1), \text{ with } \beta = \frac{eT}{bT + 1} \text{ and } \Lambda = \frac{1}{\ln(\beta + 1)}. \tag{51}$$

We therefore have

$$Q(y) = eTy^2 + bT. \tag{52}$$

and

$$P(y) = -4eT\Lambda\beta y^2 / (\beta y^2 + 1). \tag{53}$$

To solve the eigenvalue problem (43), subject to the boundary conditions (42), we applied a pseudo-spectral collocation method using Chebyshev interpolation. The

QZ algorithm was used to compute the marginal stability curve by determining the values of σ and α. The adopted procedure is implemented in MATLAB R2026a. The number of collocation points used for all results in Section 5.2 is $N = 100$. For these values ($M = 0.5$), ($\mathrm{Re} = 0.5$), ($e = 0.02$), ($b = 0.01$) and ($T = 0.5$), we obtain: for $N = 150$, $\sigma_{\max} = 1688808.640182$; for $N = 100$, $\sigma_{\max} = 381523.378317$; for $N = 80$, $\sigma_{\max} = 381523.378317$. For each value of N, $\alpha_{\min} > 0$. The code was tested by computing the eigenvalues of the Orr-Sommerfeld equation. A comprehensive description of Chebyshev spectral methods can be found in Laouer *et al.* [34], Boyd *et al.* [35], Weideman and Reddy [36], Peyret *et al.* [37], Driscoll *et al.* [38], Canuto *et al.* [39], and Motsa *et al.* [40].

5. Results and Discussions

5.1. Basic Flow

Figure 1 shows the variation of viscosity with hematocrit. It can be observed that the viscosity exhibits nearly identical behavior for the three empirical models given by Equation (25), Equation (27), and Equation (29).

Figure 2 illustrates, for each of these models, the variation of the basic flow velocity as a function of the transverse coordinate (y) in the absence of a magnetic field. The results reveal a strong consistency among the three models and are in excellent agreement with those reported by L. Fusi and A. Farina [22], who did not take the magnetic parameter into account in their analysis.

Figures 3-5 present the basic velocity profiles as functions of (y) for different values of the magnetic parameter (M), corresponding respectively to the Hatschek, Cokelet, and Nubar models. For all three models, an increase in the magnetic parameter (M) leads to a progressive reduction in the velocity near the centerline of the flow. Physically, a stronger magnetic field promotes a higher hematocrit concentration along the arterial axis, thereby increasing the blood viscosity in the central region and consequently reducing the flow velocity.

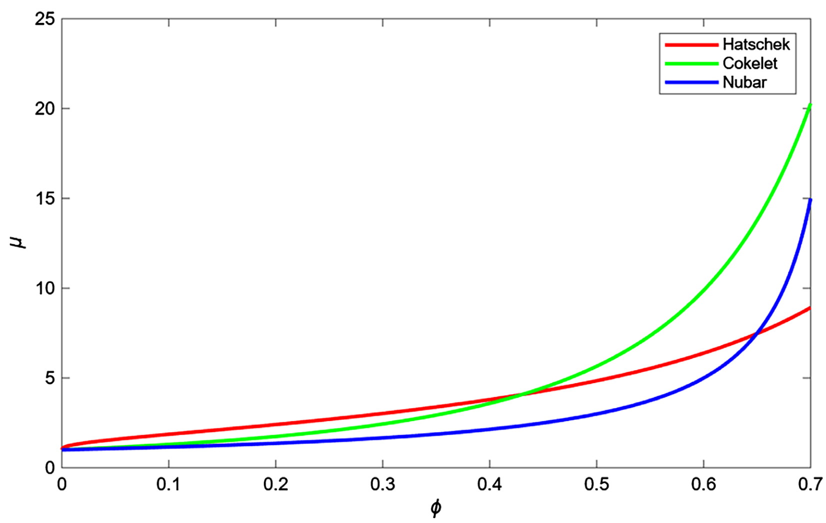

Figure 1. Example of $\mu(\phi)$.

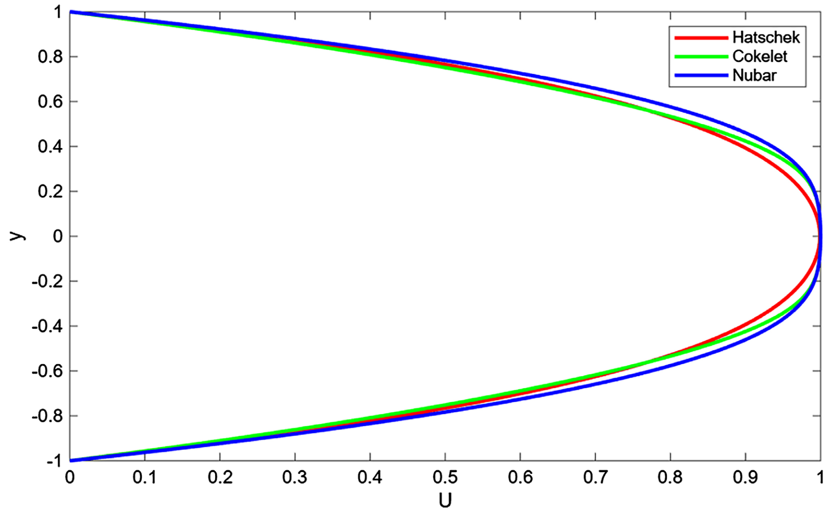

Figure 2. Corresponding velocity profiles for $M = 0$.

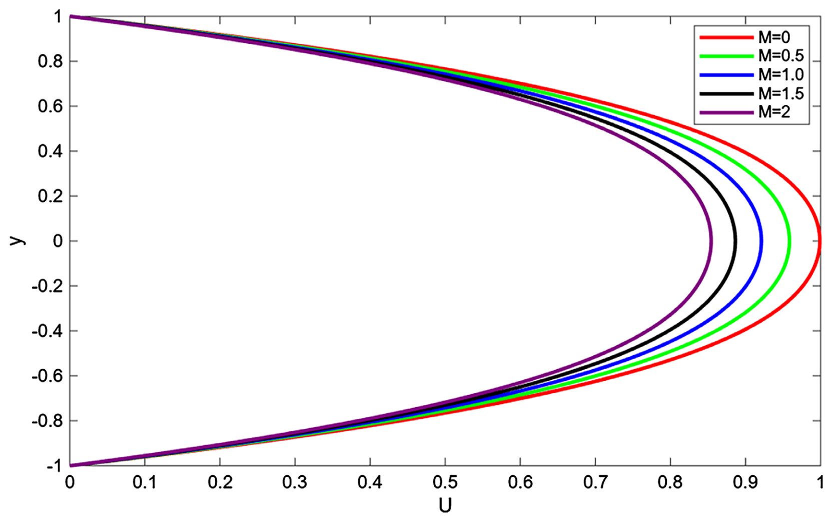

Figure 3. Hatschek modal for differnts values of M.

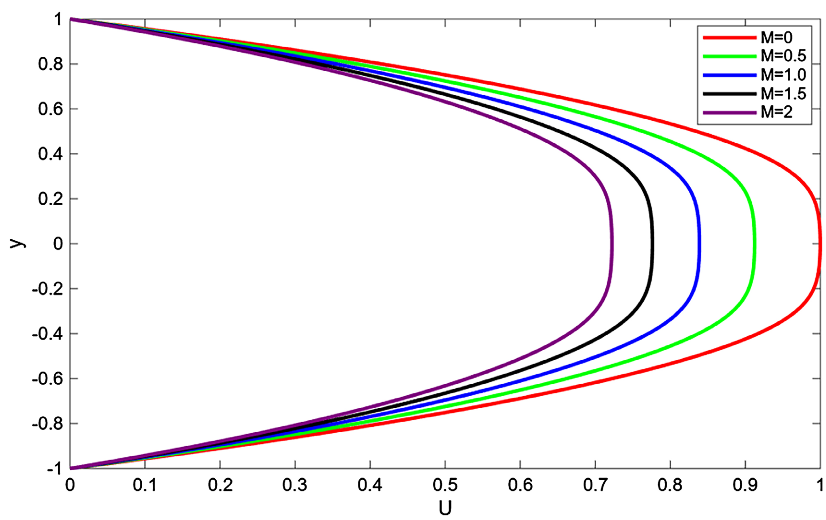

Figure 4. Cokelet modal for differnts values of M.

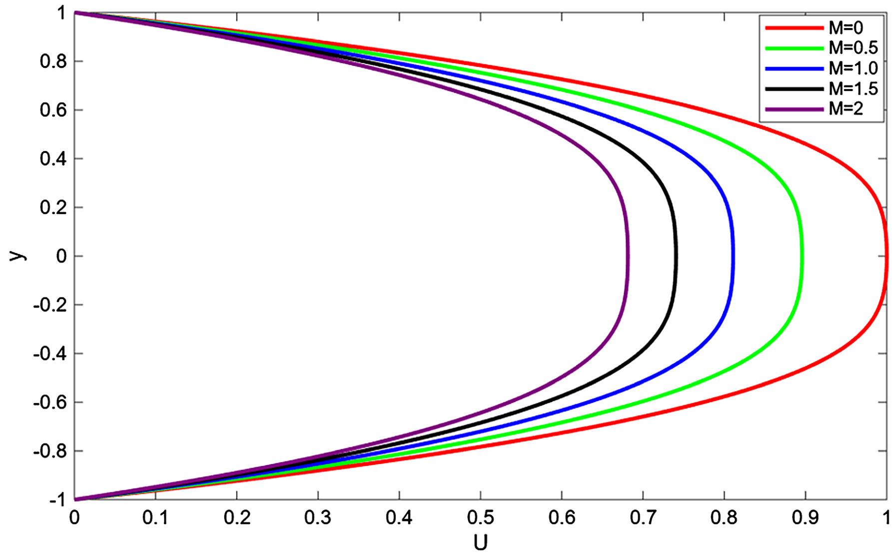

Figure 5. Nubar modal for differnts values of M.

5.2. Stability Analysis Results

The numerical results presented in this study were obtained using the Chebyshev pseudospectral collocation method implemented in MATLAB R2026a. The effects of the magnetic parameter (*M*) and the Reynolds number (Re) on the wave propagation velocity, ($c = c_r + ic_i$), the wavenumber α, and the flow frequency ω were investigated. The corresponding results are displayed in **Figures 6-13**. These stability results use the simplified test profile for hematocrit (Equation (48)), viscosity (Equation (49)) and velocity (Equation (51)). The following reference values (see [22]) were used throughout the numerical computations: ($M = 0.5$), ($\mathrm{Re} = 0.5$), ($b = 0.01$), and ($T = 0.5$). Two values of the hematocrit parameter (e) were considered: ($e = 0.02$), corresponding to an increased hematocrit concentration (or viscosity) near the channel walls, and ($e = -0.002$), corresponding to a decreased hematocrit concentration (or viscosity) near the channel walls.

In all these figures, it is observed that the growth rate σ remains positive for all values of the parameters studied-here, low parameter values ($M < 10$, $\mathrm{Re} < 10$) are used, given the context of the research (microvessels)-indicating that the perturbed flow is unconditionally unstable. Such behavior was also observed by L. Fusi and A. Farina [22].

For the default values of the parameters, σ increases rapidly for small values of α, reaches a maximum at ($\alpha = 0.0152$), and then decreases sharply, tending toward zero as α increases further. It is also noteworthy that both the corresponding frequency and the phase velocity are negative throughout the considered range of α. Moreover, the results indicate an inverse relationship between the growth rate and the frequency: as σ increases, the corresponding frequency becomes more negative. However, the peak values of σ vary significantly with the magnetic parameter M ($M = 0.5, 1.5, 3.0$ and 5.0) and the Reynolds number Re ($\mathrm{Re} = 0.5, 1.0, 2.0$ and 5.0). In the case $e > 0$, corresponding to an increasing concentration of red blood cells as y approaches the lateral walls, increasing the magnetic parameter M leads to a slight and gradual decrease in the imaginary part of the mass eigenvalue, σ, over the entire range of α (**Figure 6(a)**). Consequently, the associated frequency increases progressively (**Figure 6(b)**). Likewise, for $e > 0$, increasing the Reynolds number Re also causes a slight and gradual decrease in σ as a function of α (**Figure 7(a)**). However, unlike the magnetic parameter, the Reynolds number has virtually no influence on the corresponding frequency (**Figure 7(b)**).

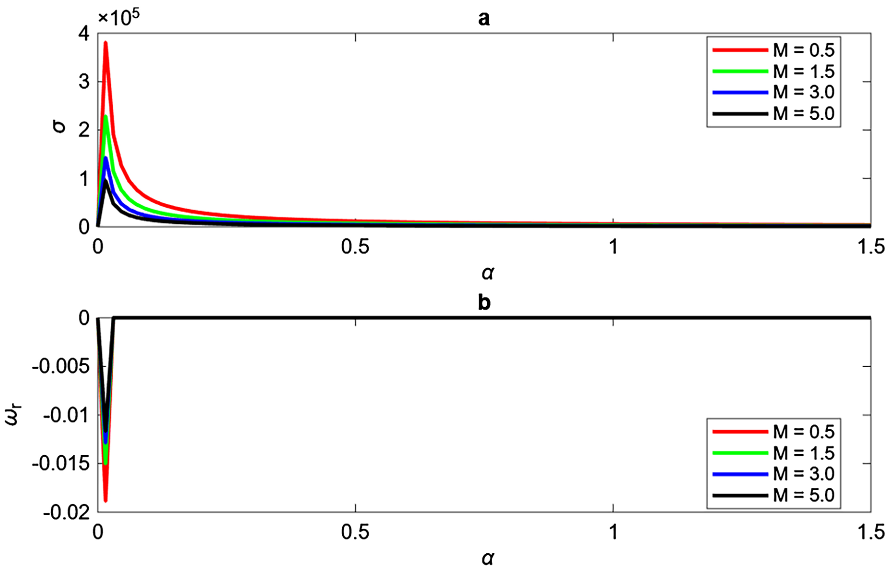

Figure 6. a) Neutral stability curves ($\sigma = \sigma(\alpha)$); b) disperssion relation; for differnts values of M with $e > 0$.

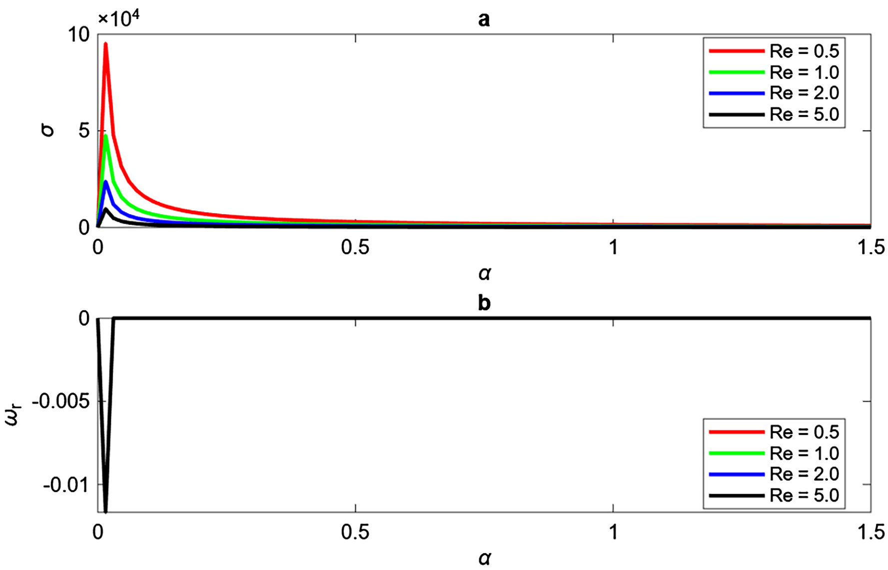

Figure 7. a) Neutral stability curves ($\sigma = \sigma(\alpha)$); b) disperssion relation; for differnts values of Re with $e > 0$.

We now examine the second case, namely $e < 0$, where the distribution of red blood cells decreases as (y) approaches the lateral walls, a behavior that is considered physically consistent according to the classical literature [1]. In this case, we again find that increasing either the magnetic parameter (M) (Figure 8(a)) or the Reynolds number (Re) (Figure 9(a)) progressively reduces the mass eigenvalues σ as a function of the wavenumber α. Consequently, the corresponding frequencies increase progressively, as shown in Figure 8(b) and Figure 9(b).

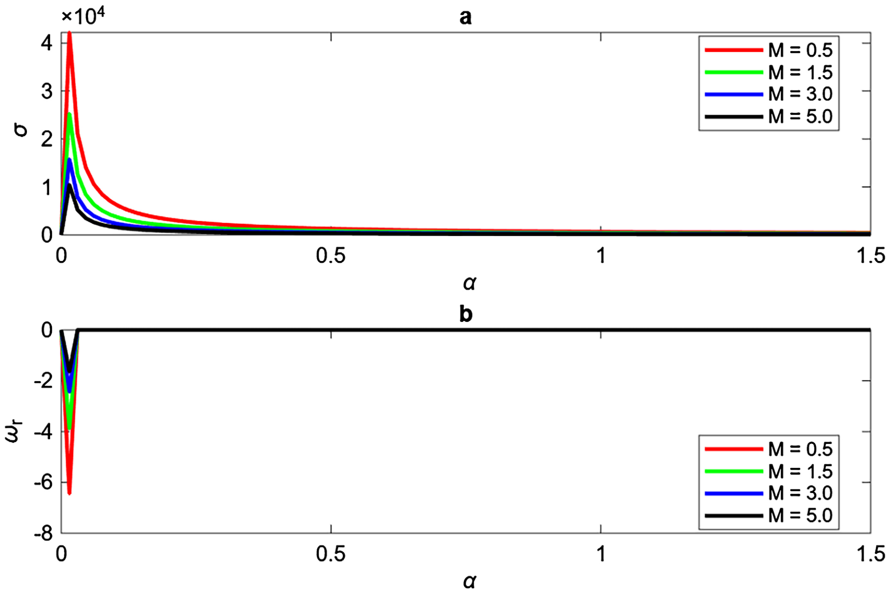

Figure 8. a) Neutral stability curves ($\sigma = \sigma(\alpha)$); b) dispersssion relation; for differnts values of M with $e < 0$.

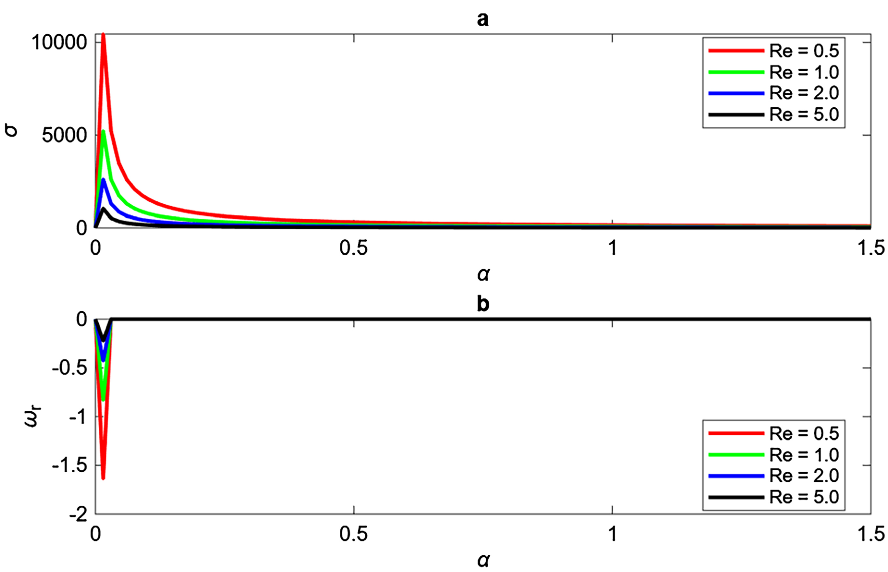

Figure 9. a) Neutral stability curves ($\sigma = \sigma(\alpha)$); b) dispersssion relation; for differnts values of Re with $b < 0$.

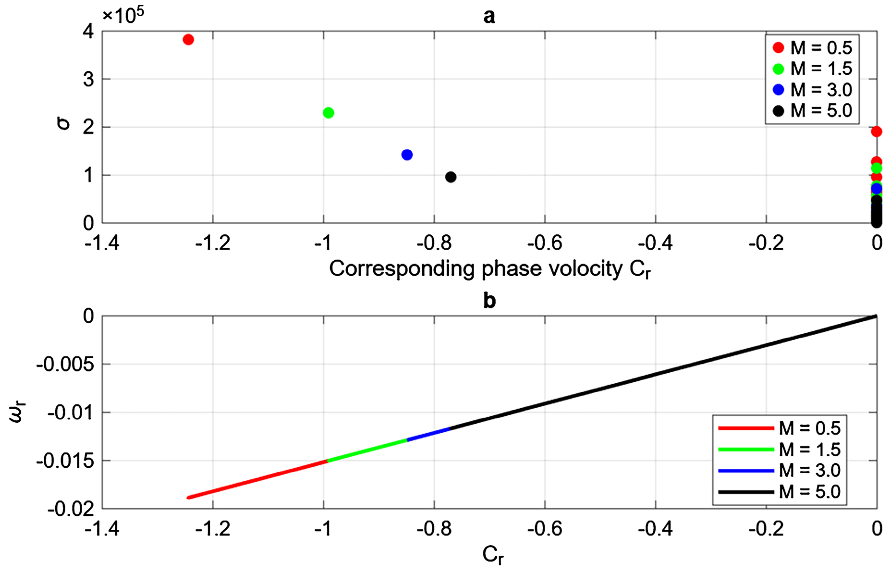

Figure 10. a) Eigenvalue spectrum ($\sigma = \sigma(C_r)$); b) dispersssion relation; for differnts values of M with $e > 0$.

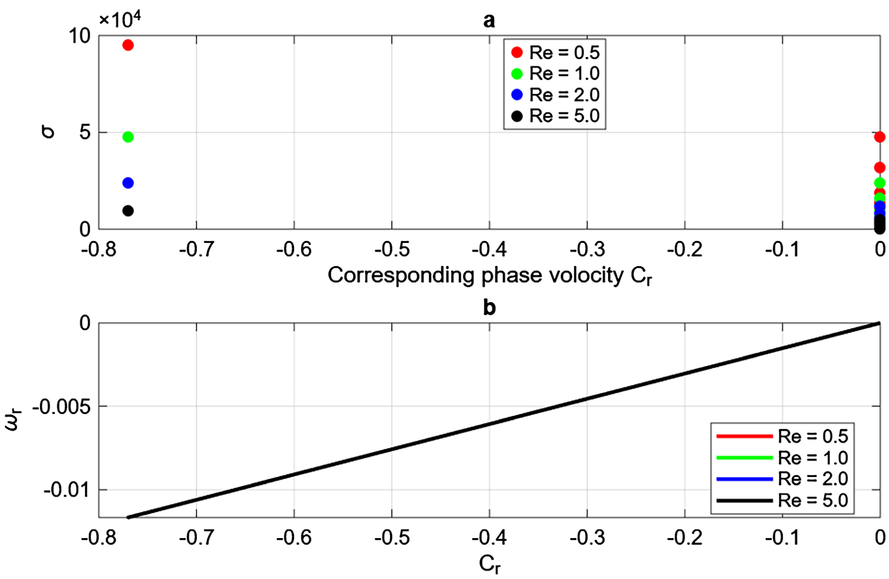

Figure 11. a) Eigenvalue spectrum ($\sigma = \sigma(C_r)$); b) dispersssion relation; for differnts values of Re with $e > 0$.

Figure 10 shows, for $e > 0$, the variation of σ as a function of the corresponding real part (phase velocity) (Figure 10(a)), together with the corresponding dispersion relation (Figure 10(b)), for different values of the magnetic parameter (M). This figure enables us to identify, for each value of (M), the most unstable modal point (Figure 10(a)) and the corresponding dispersion domain (Figure 10(b)). Similarly, Figure 11 presents, for $e > 0$, the variation of σ as a function of the corresponding real part (phase velocity) (Figure 11(a)), as well as the corresponding dispersion relation (Figure 11(b)), for different values of the Reynolds number (Re). As in Figure 10, Figure 11 illustrates, for each value of (Re), the most unstable modal point (Figure 11(a)) and the corresponding dispersion domain (Figure 11(b)). It can therefore be concluded that increasing either (M) (Figure 10) or (Re) (Figure 11) progressively decreases the growth rate associated with the most unstable modal point (Figure 10(a) and Figure 11(a), respectively).

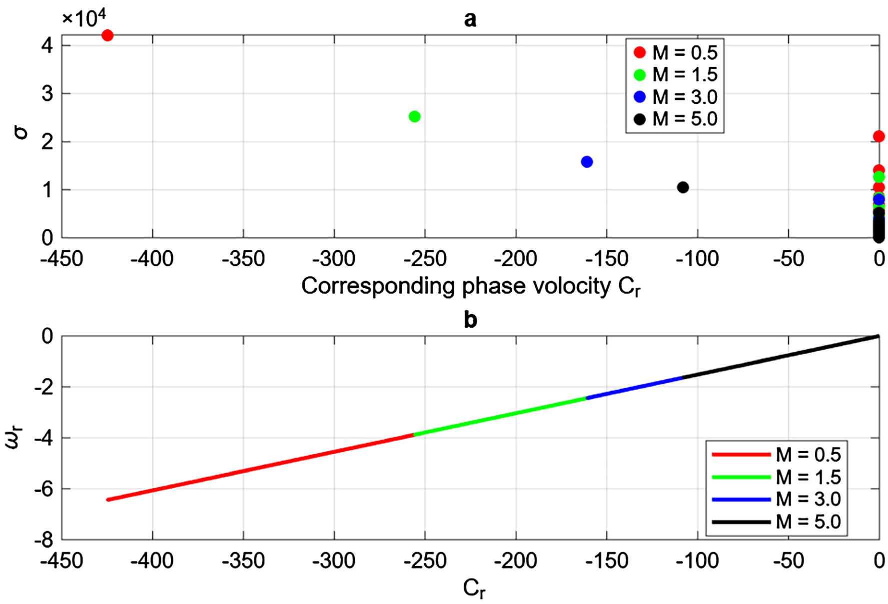

Figure 12. a) Eigenvalue spectrum ($\sigma = \sigma(C_r)$); b) dispersssion relation; for differnts values of M with $e < 0$.

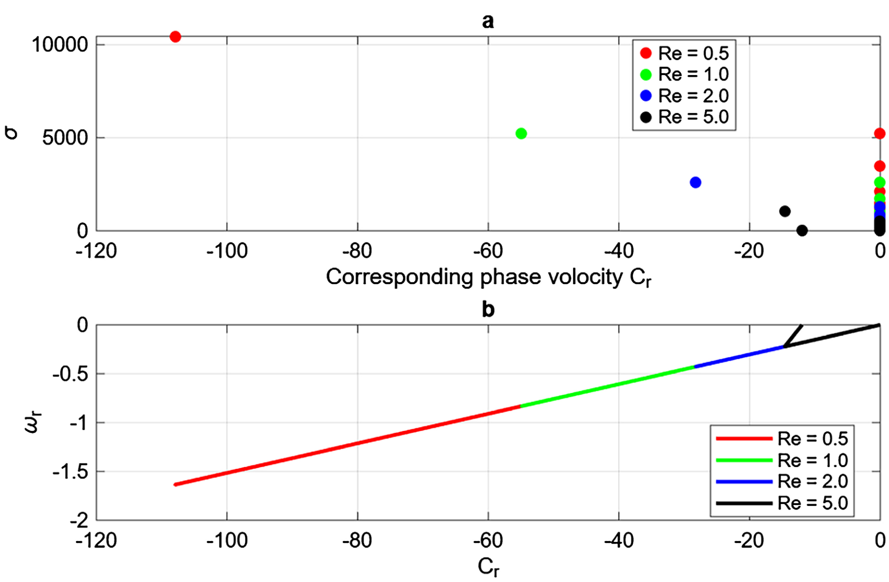

Figure 13. a) Eigenvalue spectrum ($\sigma = \sigma(C_r)$); b) dispersssion relation; for differnts values of Re with $e < 0$.

In the second case, increasing either (M) (Figure 12) or (Re) (Figure 13) progressively decreases the most unstable modal point (Figure 12(a) and Figure 13(a), respectively). The corresponding dispersion domains are illustrated in Figure 12(b) and Figure 13(b). Table 1 and Table 2 summarize the effects of (M) and (Re) on the perturbed flow for the case ($e > 0$). In particular, an increase in (M) (Table 1) or in (Re) (Table 2) leads to a decrease in the maximum growth rate, $\sigma_{\max}$. This decrease is accompanied by an increase in both the frequency and the corresponding phase velocity, while the critical wavenumber α_c remains unchanged. From these figures and tables, we conclude that the stabilization of blood flow in arteries under the influence of the magnetic parameter (M) or the Reynolds number (Re) can be attributed to the migration of red blood cells from the arterial walls toward the center as either parameter increases. Consequently, the effective viscosity decreases near the walls and increases in the core region of the artery. It is worth noting that, for $e < 0$, the stabilizing effect of increasing (M) or (Re) is more pronounced than for $e > 0$. This behavior can be explained by the hematocrit distribution: when $e < 0$, the hematocrit decreases toward the walls, whereas for $e > 0$, it increases toward the walls. Therefore, the observed instability exhibits characteristics similar to the Tollmien-Schlichting instability, which is known to originate from viscous effects near the wall. A lower viscosity in this region results in a weaker instability and, consequently, a more stable flow.

Table 1. Summary of results relating to the effect of M on the disturbed flow with $e = 0.02$.

M	$\sigma_{\max}$	α_c	ω_r	c_r
0.5	381523.378317	0.0152	−0.018863	−1.244966
1.5	228861.226980	0.0152	−0.015023	−0.991506
3.0	142988.766836	0.0152	−0.012866	−0.849164
5.0	95281.844543	0.0152	−0.011672	−0.770378

Table 2. Summary of results relating to the effect of Re on the disturbed flow with $e = 0.02$.

Re	$\sigma_{\max}$	α_c	ω_r	c_r
0.5	381523.378317	0.0152	−0.018863	−1.244966
1.0	190761.689170	0.0152	−0.018863	−1.244958
2.0	95380.844594	0.0152	−0.018863	−1.244955
5.0	38152.337850	0.0152	−0.018863	−1.244960

6. Conclusion

In this study, we investigated the linear temporal stability of a unidirectional plane Poiseuille blood flow modeled as an inhomogeneous fluid subjected to the combined effects of the magnetic parameter and the Reynolds number. The fluid viscosity was assumed to depend on the hematocrit distribution. The basic flow was assumed to be laminar and two-dimensional. Three empirical viscosity laws, expressed as functions of hematocrit, were considered. For each model, the corresponding basic velocity profile in the presence of a magnetic field was computed numerically using the BVP4C solver in Matlab. For the perturbed flow, the viscosity was expressed as a function of hematocrit, leading to two distinct configurations. In the first configuration (Case 1), the hematocrit increases from the centerline toward the vessel wall, whereas in the second configuration (Case 2), it exhibits the opposite trend. The stability of the system was analyzed using the classical normal-mode approach. The resulting polynomial eigenvalue problem was solved numerically using Chebyshev pseudo-spectral collocation, implemented in MATLAB. The numerical results indicate that, for all rheological models considered, the flow is unconditionally unstable in both Case 1 and Case 2. Nevertheless, despite this unconditional instability, our results show that increasing either the magnetic parameter or the Reynolds number reduces the growth rate of the instability in both configurations. This stabilizing effect is of particular interest in hemodynamics, as it may help protect the vascular walls from excessive mechanical stress.

Acknowledgements

The authors would like to thank the reviewers of this paper for their valuable contributions.

Funding Declaration

The authors declare that no funding was obtained for the production of this manuscript.

Author Contributions

T.F.L., H.S., K.P.M. and A.L. established the equations; T.F.L., H.S. and A.L. prepared all the figures; T.F.L., H.S. and A.L. wrote the manuscript and all the authors revised the manuscript.

Conflicts of Interest

The authors declare no conflicts of interest regarding the publication of this paper.

References

[1] Haynes, R.H. (1960) Physical Basis of the Dependence of Blood Viscosity on Tube Radius. *American Journal of Physiology-Legacy Content*, **198**, 1193-1200. https://doi.org/10.1152/ajplegacy.1960.198.6.1193

[2] Moyers-Gonzalez, M., Owens, R.G. and Fang, J. (2008) A Non-Homogeneous Constitutive Model for Human Blood. Part 1. Model Derivation and Steady Flow. *Journal of Fluid Mechanics*, **617**, 327-354. https://doi.org/10.1017/s002211200800428x

[3] Ascolese, M., Farina, A. and Fasano, A. (2019) The Fåhræus-Lindqvist Effect in Small Blood Vessels: How Does It Help the Heart? *Journal of Biological Physics*, **45**, 379-394. https://doi.org/10.1007/s10867-019-09534-4

[4] Fournier, R.L. (2012) Basic Transport in Biomedical Engineering. CRC. https://archive.org/details/basictransportph0000four_c7g8_3ed/page/468/mode/1up

[5] Anand, M. and Rajapola, K. (2005) A Note on the Flows of Inhomogeneous Fluids with Shear-Dependent Viscosities. *Archives of Mechanics*, **57**, 417-428. https://am.ippt.gov.pl/index.php/am/article/view/v57p417/pdf

[6] Hickox, C.E. (1971) Instability Due to Viscosity and Density Stratification in Axisymmetric Pipe Flow. *The Physics of Fluids*, **14**, 251-262. https://doi.org/10.1063/1.1693422

[7] Preziosi, L., Chen, K. and Joseph, D.D. (1989) Lubricated Pipelining: Stability of Core-Annular Flow. *Journal of Fluid Mechanics*, **201**, 323-356. https://doi.org/10.1017/s0022112089000960

[8] Anand, M., Kiranmai, P. and Garimella, S.M. (2024) Stability of Fully Developed Pipe Flow of a Shear-Thinning Fluid That Approximates the Response of Viscoplastic Fluids. *Applications in Engineering Science*, **19**, Article 100191. https://doi.org/10.1016/j.apples.2024.100191

[9] Fang, J. and Owens, R.G. (2006) Numerical Simulations of Pulsatile Blood Flow Using a New Constitutive Model. *Biorheology*, **43**, 637-660. https://doi.org/10.1177/0006355x2006043005001

[10] Owens, R.G. (2006) A New Microstructure-Based Constitutive Model for Human Blood. *Journal of Non-Newtonian Fluid Mechanics*, **140**, 57-70. https://doi.org/10.1016/j.jnnfm.2006.01.015

[11] Fusi, L. (2018) Two-Dimensional Thin-Film Flow of an Incompressible Inhomogeneous Fluid in a Channel. *Journal of Non-Newtonian Fluid Mechanics*, **260**, 87-100. https://doi.org/10.1016/j.jnnfm.2018.07.001

[12] Massoudi, M., Kim, J. and Antaki, J.F. (2012) Modeling and Numerical Simulation of Blood Flow Using the Theory of Interacting Continua. *International Journal of Non-Linear Mechanics*, **47**, 506-520. https://doi.org/10.1016/j.ijnonlinmec.2011.09.025

[13] Fusi, L., Farina, A., Rosso, F. and Rajagopal, K. (2019) Thin-Film Flow of an Inhomogeneous Fluid with Density-Dependent Viscosity. *Fluids*, **4**, Article 30. https://doi.org/10.3390/fluids4010030

[14] Fasano, A. and Sequeira, A. (2017) Hemomath: The Mathematics of Blood. Springer. https://link.springer.com/book/10.1007/978-3-319-60513-5

[15] Khan, A., Zaman, G., Li, Y., Ahmad, S. and Hussain, A. (2017) The Oscillatory Motion of Oldroyd-B Fluid by Incorporating Some of the Mechanical Factors. *Journal of Applied Mathematics and Physics*, **5**, 2402-2410. https://doi.org/10.4236/jamp.2017.512196

[16] Papalexandris, M.V. (2004) A Two-Phase Model for Compressible Granular Flows Based on the Theory of Irreversible Processes. *Journal of Fluid Mechanics*, **517**, 103-112. https://doi.org/10.1017/s0022112004000874

[17] Varsakelis, C. and Papalexandris, M.V. (2011) Low-Mach-Number Asymptotics for Two-Phase Flows of Granular Materials. *Journal of Fluid Mechanics*, **669**, 472-497. https://doi.org/10.1017/s0022112010005173

[18] Goldsmith, H.L. and Marlow, J.C. (1979) Flow Behavior of Erythrocytes. II. Particle Motions in Concentrated Suspensions of Ghost Cells. *Journal of Colloid and Interface Science*, **71**, 383-407. https://doi.org/10.1016/0021-9797(79)90248-0

[19] Moyers-Gonzalez, M.A. and Owens, R.G. (2010) Mathematical Modelling of the Cell-Depleted Peripheral Layer in the Steady Flow of Blood in a Tube. *Biorheology*, **47**, 39-71. https://doi.org/10.3233/bir-2010-0558

[20] Dimakopoulos, Y., Kelesidis, G., Tsouka, S., Georgiou, G.C. and Tsamopoulos, J. (2015) Hemodynamics in Stenotic Vessels of Small Diameter under Steady State Con-

ditions: Effect of Viscoelasticity and Migration of Red Blood Cells. *Biorheology*, **52**, 183-210. https://doi.org/10.3233/bir-14033

[21] Coupier, G., Kaoui, B., Podgorski, T. and Misbah, C. (2008) Non-Inertial Lateral Migration of Vesicles in Bounded Poiseuille Flow. *Physics of Fluids*, **20**, Article 111702. https://doi.org/10.1063/1.3023159

[22] Fusi, L. and Farina, A. (2020) Linear Stability Analysis of Blood Flow in Small Vessels. *Applications in Engineering Science*, **1**, Article 100002. https://doi.org/10.1016/j.apples.2020.100002

[23] Lihonou, T.F., Monwanou, A.V., Miwadinou, C.H. and Orou, J.B.C. (2022) Active Control of the Instability of a Dynamic Laminar Boundary Layer on a Flat Impermeable Plate Subjected to a Magnetic Field. *Indian Journal of Physics*, **96**, 3591-3601. https://doi.org/10.1007/s12648-022-02284-5

[24] John, M.O., Obrist, D. and Kleiser, L. (2015) Stabilizing a Leading-Edge Boundary Layer Subject to Wall Suction by Increasing the Reynolds Number. *Procedia IUTAM*, **14**, 394-402. https://doi.org/10.1016/j.piutam.2015.03.065

[25] Lebbal, S. (2022) Dynamics of Pulsed Flows in Deformable Channels. University of Lyon. (In Français) https://theses.hal.science/tel-03577495v1

[26] Hund, S.J., Kameneva, M.V. and Antaki, J.F. (2017) A Quasi-Mechanistic Mathematical Representation for Blood Viscosity. *Fluids*, **2**, 10-36. https://doi.org/10.3390/fluids2010010

[27] Hatschek, E. (1920) Eine Reihe von abnormen Liesegang'schen Schichtungen. *Kolloid-Zeitschrift*, **27**, 225-229. https://doi.org/10.1007/bf01427700

[28] Cokelet, G.R. (1963) The Rheology of Human Blood. Doctoral Dissertation, Massachusetts Institute Technology. https://dspace.mit.edu/entities/publication/ca65fc8d-5307-4f81-a2af-283b46698659

[29] Nubar, Y. (1967) Effect of Slip on the Rheology of a Composite Fluid: Application to Blood. *Biorheology*, **4**, 133-150. https://doi.org/10.3233/bir-1967-4401

[30] Shampine, L., Kierzenka, J. and Reichelt, M. (2000) Solving Boundary Value Problems for Ordinary Differential Equations in MATLAB with bvp4c. Tutorial Notes, 1-27. https://share.google/kQ4RcRzPotyDwbDTA

[31] Jamir, T. and Konwar, H. (2022) Effects of Radiation Absorption, Soret and Dufour on Unsteady MHD Mixed Convective Flow Past a Vertical Permeable Plate with Slip Condition and Viscous Dissipation. *Journal of Heat and Mass Transfer Research*, **9**, 155-168. https://doi.org/10.22075/jhmtr.2023.28693.1399

[32] Lihonou, T.F., Laouer, A., Mathos, K.P. and Yombouno, F.M. (2025) Analysis of Heat and Mass Transfer in MHD Free Convection with Chemical Reaction Effects on a Moving Vertical Porous Plate. *Open Journal of Fluid Dynamics*, **15**, 87-115. https://doi.org/10.4236/ojfd.2025.152006

[33] Lihonou, T.F., Diakite, M., Laouer, A., Segning, H., Mathos, K.P. and Camara, N. (2025) Analysis of Heat and Mass Transfer in MHD Forced Convection with Chemical Parameter Effects on a Horizontal Porous Plate. *Brazilian Journal of Physics*, **55**, Article No. 275. https://doi.org/10.1007/s13538-025-01907-6

[34] Laouer, A., Mezaache, E.H. and Laouar, S. (2016) Influence of Surface Mass Transfer on the Stability of Forced Convection Flow over a Horizontal Flat Plate. *Computational Thermal Sciences: An International Journal*, **8**, 355-369. https://doi.org/10.1615/computthermalscien.2016016415

[35] Boyd, J.P. (2000) Chebyshev and Fourier Spectral Methods. Dover Publications. https://share.google/eeRD1nhvWorW0Jgy5

[36] Weideman, J.A. and Reddy, S.C. (2000) A MATLAB Differentiation Matrix Suite. *ACM Transactions on Mathematical Software*, **26**, 465-519. https://doi.org/10.1145/365723.365727

[37] Peyret, R. (2002) Spectral Methods for Incompressible Viscous Flow. Springer.

[38] Driscoll, T.A., Hale, N. and Trefethen, L.N. (2014) Chebfun Guide. Pafnuty Publications.

[39] Canuto, C., Hussaini, M.Y., Quarteroni, A. and Zang, T.A. (1988) Spectral Methods in Fluid Dynamics. Springer. https://link.springer.com/book/10.1007/978-3-642-84108-8

[40] Motsa, S.S., Marewo, G.T., Sibanda, P. and Shateyi, S. (2011) An Improved Spectral Homotopy Analysis Method for Solving Boundary Layer Problems. *Boundary Value Problems*, **2011**, Article No. 3. https://doi.org/10.1186/1687-2770-2011-3

Nomenclature

B_0	Magnetic component ($Wb \cdot m^{-2}$)
b	relative thickness of the layer
$c = c_r + ic_i$	the wave velocity (complex eigenvalue)
c_r	phase velocity
$D = \frac{\partial}{\partial y}$	the Chebyshev spectral differentiation matrix
e	red blood cell concentration
E	The electric field
f	associated eigenfunction
G^o	dimensional pressure gradient
G	dimensionless pressure gradient
H^o	Amplitude
J	The current density vector
L^o	Plate length or maximum value of x
M	Magnetic parameter
p^o	Dimensional pressure
p	Dimensionless pressure
R_e	the Reynolds number
t^o	time dimensional
t	time non-dimensional
T	viscosity ratio
$\hat{u}$, $\hat{v}$, $\hat{p}$, $\hat{\phi}$	the fluctuating components for the perturbations u, v, p and ϕ respectively
U	Dimensionless primary velocity
U^o	Uniform velocity (m/s)
u^o, v^o	Velocity (m/s)
U, V	Dimensionless velocity components
x^o, y^o	Dimensional cartesian coordinates (m)
x, y	Dimensionless cartesian coordinates

Greek Symbols

α	wave number
α_c	critical wave number
ω_r	Frequency
ϕ	Hematocrit function
ρ^o	Fluid density (kg·m^{-3})
∇	Nabla operator
Γ_j	the differential operators
σ	Unstable mode
$\sigma_{\max}$	Unstable mode
μ_p^o	Reference viscosity, (Pa·s)
μ^o	Dynamic viscosity, (Pa·s)
$\mu(\phi)$	dimensionless dynamic viscosity
μ_e	The magnetic permeability
ε_e	Absolute permittivity of the fluid
λ	The fluid electrical conductivity

Appendix

We provide here the coefficients introduced in (b18).

$$\Gamma_{00}(y) = -Q\left(\frac{\mathrm{d}^4U}{\mathrm{d}y^4}\right) - \frac{\mathrm{d}^4U}{\mathrm{d}y^4} - 2\left(\frac{\mathrm{d}Q}{\mathrm{d}y}\right)\left(\frac{\mathrm{d}^3U}{\mathrm{d}y^3}\right) + 2Q\alpha^2\left(\frac{\mathrm{d}^2U}{\mathrm{d}y^2}\right)$$
$$+2\alpha^2\left(\frac{\mathrm{d}^2U}{\mathrm{d}y^2}\right) - \left(\frac{\mathrm{d}^2Q}{\mathrm{d}y^2}\right)\left(\frac{\mathrm{d}^2U}{\mathrm{d}y^2}\right) + 2\left(\frac{\mathrm{d}Q}{\mathrm{d}y}\right)\alpha^2\left(\frac{\mathrm{d}U}{\mathrm{d}y}\right) - i\,\mathrm{Re}\,\alpha^3U^2$$
$$-Q\alpha^4U - \alpha^4U - \left(\frac{\mathrm{d}^2Q}{\mathrm{d}y^2}\right)\alpha^2U - P\alpha^2 - \frac{\mathrm{d}^2P}{\mathrm{d}y^2} + M\left(\frac{\mathrm{d}^2U}{\mathrm{d}y^2}\right),$$

$$\Gamma_{01}(y) = -4Q\left(\frac{\mathrm{d}^3U}{\mathrm{d}y^3}\right) - 4\left(\frac{\mathrm{d}^3U}{\mathrm{d}y^3}U\right) - 6\left(\frac{\mathrm{d}Q}{\mathrm{d}y}\right)\left(\frac{\mathrm{d}^2U}{\mathrm{d}y^2}\right) + 2i\,\mathrm{Re}\,\alpha U\left(\frac{\mathrm{d}U}{\mathrm{d}y}\right)$$
$$+4Q\alpha^2\left(\frac{\mathrm{d}U}{\mathrm{d}y}\right) + 4a^2\left(\frac{\mathrm{d}U}{\mathrm{d}y}\right) - 2\left(\frac{\mathrm{d}^2Q}{\mathrm{d}y^2}\right)\left(\frac{\mathrm{d}U}{\mathrm{d}y}\right) + 2\left(\frac{\mathrm{d}Q}{\mathrm{d}y}\right)\alpha^2U$$
$$-2\left(\frac{\mathrm{d}P}{\mathrm{d}y}\right) + 2M\left(\frac{\mathrm{d}U}{\mathrm{d}y}\right),$$

$$\Gamma_{02}(y) = -6Q\left(\frac{\mathrm{d}^2U}{\mathrm{d}y^2}\right) - 6\left(\frac{\mathrm{d}^2U}{\mathrm{d}y^2}\right) - 6\left(\frac{\mathrm{d}Q}{\mathrm{d}y}\right)\left(\frac{\mathrm{d}U}{\mathrm{d}y}\right) + i\,\mathrm{Re}\,\alpha U^2$$
$$+2Q\alpha^2U + 2\alpha^2U - \left(\frac{\mathrm{d}^2Q}{\mathrm{d}y^2}\right)U - P + MU,$$

$$\Gamma_{03}(y) = -4Q\left(\frac{\mathrm{d}U}{\mathrm{d}y}\right) - 4\left(\frac{\mathrm{d}U}{\mathrm{d}y}\right) - 2\left(\frac{\mathrm{d}Q}{\mathrm{d}y}\right)U,$$

$$\Gamma_{04}(y) = -(Q+1)U.$$

$$\Gamma_{10}(y) = 2i\,\mathrm{Re}\,\alpha^3U + Q\alpha^4 + \alpha^4 + \left(\frac{\mathrm{d}^2Q}{\mathrm{d}y^2}\right)\alpha^2,$$

$$\Gamma_{11}(y) = -2i\,\mathrm{Re}\,\alpha\left(\frac{\mathrm{d}U}{\mathrm{d}y}\right) - 2\left(\frac{\mathrm{d}Q}{\mathrm{d}y}\right)a^2,$$

$$\Gamma_{12}(y) = -2i\,\mathrm{Re}\,\alpha U - 2Q\alpha^2 - 2\alpha^2 + \frac{\mathrm{d}^2Q}{\mathrm{d}y^2} - M,$$

$$\Gamma_{13}(y) = 2\left(\frac{\mathrm{d}Q}{\mathrm{d}y}\right),$$

$$\Gamma_{14}(y) = Q+1.$$

$$\Gamma_{20}(y) = -i\,\mathrm{Re}\,\alpha^3,\ \Gamma_{21} = 0,\ \Gamma_{22} = i\,\mathrm{Re}\,\alpha,\ \Gamma_{23} = \Gamma_{24} = 0.$$